Thermophysical properties of warm dense hydrogen using quantum molecular dynamics simulations

Bastian Holst and Ronald Redmer
Institut für Physik, Universität Rostock, D-18051 Rostock, Germany

Michael P. Desjarlais
Pulsed Power Sciences Center, Sandia National Laboratories, Albuquerque, New Mexico 87185-1186, USA
(Received 2 October 2007; revised manuscript received 25 February 2008; published 9 May 2008)

We study the thermophysical properties of warm dense hydrogen by using quantum molecular dynamics simulations. Results are presented for the pair distribution functions, the equation of state, and the Hugoniot curve. From the dynamic conductivity, we derive the dc electrical conductivity and the reflectivity. We compare with available experimental data and predictions of the chemical picture. In particular, we discuss the nonmetal-to-metal transition, which occurs at about 40 GPa in the dense fluid.

DOI: 10.1103/PhysRevB.77.184201 PACS number(s): 61.20.Ja, 31.15.A−, 64.30.−t, 71.30.+h

I. INTRODUCTION

Hydrogen is an essential element for models of stellar and planetary interiors.[1,2] The isotopes deuterium and tritium are considered as target materials (D-T gas) in inertial confinement fusion experiments.[3] Therefore, numerous efforts have been made both experimentally and theoretically to understand the behavior of hydrogen, deuterium, and tritium in a wide range of densities and temperatures. In particular, progress in shock-wave experimental technique has allowed the systematic probing of the megabar pressure range, so that a sound database has been assembled within the past decade. Single or multiple shock-wave experiments have been performed for hydrogen (or deuterium) by using, e.g., high explosives (HEs),[4] gas guns,[5] pulsed power,[6–8] or high-power lasers.[9] The combination of high pressures and temperatures of several eV defines *warm dense matter*, which is a strongly correlated state relevant for planetary interiors that is characterized by partial ionization wherein the bound states exhibit a highly transient nature.

Furthermore, the enormous progress in computer capacity has allowed the development and application of *ab initio* simulation techniques for warm dense matter such as path integral Monte Carlo[10,11] (PIMC) or quantum molecular dynamics (QMD) simulations,[12,13] which systematically treat quantum effects and correlations. These techniques give already highly predictive results for a variety of problems and systems.

The equation of state (EOS) and derived quantities, such as the Hugoniot curve and the sound velocity, are important material properties in this context. Furthermore, optical properties such as, e.g., the reflectivity are closely related to the dielectric function, which also determines the dc electrical conductivity in the static limit. All these quantities are used to characterize the unique behavior of warm dense hydrogen, especially for high pressures at, or exceeding, 1 Mbar, where a transition from a nonconducting molecular fluid to a monatomic fluid with metalliclike conductivity occurs. By describing the disordered fluid in terms of solid state parameters, the fundamental band gap between the valence and conduction bands decreases with the pressure and, subsequently, the electrical conductivity shows an exponential increase as is typical of thermally activated transport in semiconductors.[14] For pressures above 1.4 Mbar, conductivities of about 2000 $\Omega^{-1}\,\mathrm{cm}^{-1}$, as is characteristic of simple metallic fluids such as Cs, have been experimentally observed at around 3000 K (Refs. 15 and 16) and band gap closure has been claimed to be responsible for this nonmetal-to-metal transition.

On the other hand, concepts of plasma physics have been applied to warm dense matter states.[17] For instance, the chemical picture gives a rather simple description by identifying stable bound states out of elementary particles as new composite particles. Hydrogen at normal conditions in this context is a molecular fluid. Free electrons are generated at high pressure by dissociation of molecules, $H_2 \rightleftharpoons 2H$, and a subsequent ionization of atoms, $H \rightleftharpoons e+p$. This model already yields a strong increase in conductivity with pressure (pressure ionization). In addition, bound states contribute to conduction via hopping processes.[18] The conceptual problem of all chemical models is the clear definition of bound states, the derivation of effective potentials between all species, and the calculation of cross sections for the respective scattering processes in a strongly correlated medium.

QMD simulations are a powerful tool to describe warm dense matter.[19–28] The combination of classical molecular dynamics for the ions and density functional theory (DFT) for the electrons allows one to consider correlation and quantum effects. Alternatively, wave packet molecular dynamics (WPMD) simulations were developed, in which the electrons are represented on a semiquantal level by wave packets.[29–34]

In this paper, we apply QMD simulations and calculate a broad spectrum of thermophysical properties of warm dense hydrogen. We determine EOS data for a wide region of densities and temperatures and compare them with chemical models. We calculate the principal Hugoniot curve for liquid targets. The Kubo–Greenwood formula serves as a starting point for the evaluation of the dynamic conductivity $\sigma(\omega)$ from which the dielectric function $\varepsilon(\omega)$, the reflectivity, and the dc conductivity can be extracted. In addition, the electronic structure calculation within DFT yields the charge density distribution in the simulation box at every time step,

 ©2008 The American Physical Society

and the molecular dynamics run gives valuable structural information via the ion-ion pair correlation function. This is important for the identification and characterization of phase transitions such as solid-liquid or liquid-plasma as well as for the nonmetal-to-metal transition.

II. QUANTUM MOLECULAR DYNAMICS SIMULATIONS

Within QMD simulations, we perform molecular dynamics simulations with a quantum mechanical treatment of the electrons by using efficient codes based on DFT (see Ref. 35). DFT is built on the theorems of Hohenberg and Kohn[36] and gives the electron density that minimizes the ground state energy of the system. It has been proven that this density is a unique functional of the effective potential V_{eff}.

From this formalism, Kohn and Sham[37] derived a computational scheme that solves the problem for a fictitious system of noninteracting particles that leads to the same electron density. This scheme basically consists of solving the following Kohn–Sham equations:

$$\left[-\frac{\hbar^2}{2m}\nabla^2 + V_{\text{eff}}(r)\right]\varphi_k(r) = \epsilon_k\varphi_k(r),$$

$$V_{\text{eff}}[\varrho(\mathbf{r})] = \int \frac{\varrho(\mathbf{r}')e^2}{|\mathbf{r}-\mathbf{r}'|}d\mathbf{r}' - \sum_{k=1}^{N}\frac{Z_k e^2}{|\mathbf{r}-\mathbf{R}_k|} + V_{\text{XC}}[\varrho(\mathbf{r})]. \tag{1}$$

Our *ab initio* quantum molecular dynamics simulations were performed within Mermin's finite temperature DFT,[38] which is implemented in the plane wave density functional code Vienna *ab initio* simulation package (VASP).[39–41] We used the projector augmented wave potentials[42] and did a generalized gradient approximation (GGA) by using the parametrization of Perdew *et al.*[43] Extensive test calculations, as performed already by Desjarlais,[22] showed that the EOS data are dependent on the plane wave cutoff. A convergence of better than 1% is secured for $E_{\text{cut}}=1200$ eV, which was used in all actual calculations. The electronic structure calculations were performed for a given array of ion positions, which are subsequently varied by the forces obtained within the DFT calculations via the Hellmann–Feynman theorem for each molecular dynamics step. This schema is repeated until the EOS measures are converged and a thermodynamic equilibrium is reached.

The simulations were done for 64 atoms in a supercell with periodic boundary conditions. The temperature of the ions was controlled by a Nosé thermostat[44] and the temperature of the electrons was fixed by Fermi weighting the occupation of bands.[40] The Brillouin zone was sampled by evaluating the results at Baldereschi's mean value point,[45] which showed the best agreement with a sampling of the Brillouin zone by using a higher number of **k** points. The density of the system was fixed by the size of the simulated supercell. To achieve a small statistical error due to fluctuations, the system was simulated 1000–1500 steps further after reaching thermodynamic equilibrium. The EOS data and pair correlation functions were then obtained by averaging over all particles and simulation steps in equilibrium. Similar calculations were recently performed for the thermophysical properties of warm dense helium[46] to verify the nonmetal-to-metal transition at high pressures.

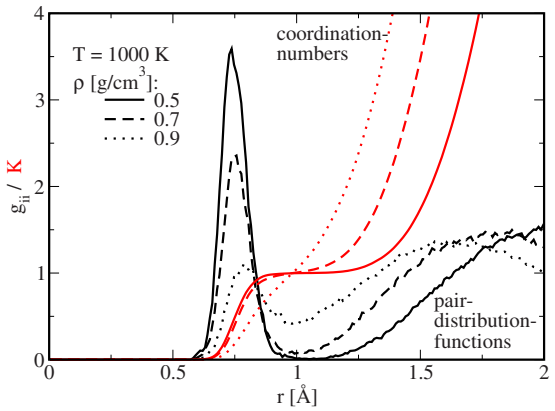

FIG. 1. (Color online) Proton-proton pair distribution function and corresponding coordination numbers according to Eq. (2) for 1000 K and three densities.

The zero-point vibrational energy of the H_2 molecules is not included in DFT calculations. In previous calculations, the energy $\frac{1}{2}h\nu_{\text{vib}}$ per molecule is simply added, which is very important, especially at low temperatures and for the calculation of an exact initial internal energy for the reference state of the Hugoniot curve, which is 0.0855 g/cm^3 at 20 K. To more sensitively account for this quantum effect for arbitrary temperatures, the fraction of molecules has to be derived, e.g., for all states along the Hugoniot curve. This can be done via the coordination number as follows:

$$K(r) = \frac{N-1}{V}\int_0^r 4\pi r'^2 g(r')dr', \tag{2}$$

which is a weighted integral over the pair correlation function $g(r)$ of the ions. N denotes the number of ions and V the volume of the supercell in the simulation. The doubled value of K at the maximum of the molecular peak in $g(r)$, which is found at around $r=0.748$ Å, is then equal to the fraction of ions bound to a molecule and is twice the amount of molecules in the supercell. An example is shown in Fig. 1, where an increase in dissociation at higher density can be seen. In Fig. 2, we show the thermal dissociation; the molecular peak disappears with increasing temperature at constant density. Note that the peak is thermally broadened.

The dissociation degree is calculated for a number of isotherms and the results are approximated by a Fermi function with two adjustable parameters. These are represented by temperature-dependent functions so that the dissociation degree and, subsequently, the contribution of molecules to the zero-point internal energy are determined for arbitrary temperatures. The results show that molecules can be neglected above 10 000 K.

We compare the resulting dissociation degree with that derived by Vorberger *et al.*[23] in Fig. 3. They counted all pairs of atoms in a range of $1.8a_B$ as atoms. In a second step, they reduced the number of molecules by counting only those

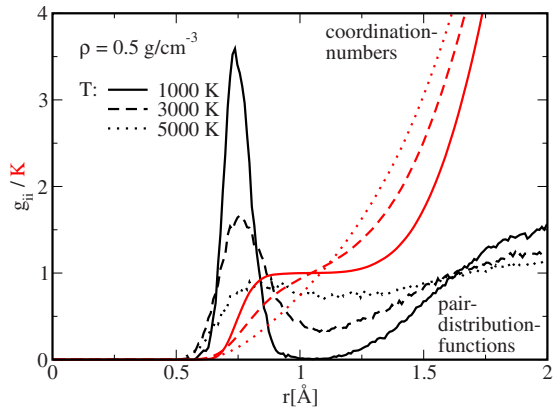

FIG. 2. (Color online) Proton-proton pair distribution function and corresponding coordination numbers according to Eq. (2) for 0.5 g/cm^3 and three temperatures.

pairs that are stable for longer than ten vibrational periods. In all three cases, the amount of molecules is lower for higher densities and the molecules disappear at higher temperatures due to thermal dissociation. This picture shows that the dissociation degree strongly depends on the definition of the term *molecule* in the warm dense matter region. Our method gives a smoother behavior of the dissociation degree, which starts at lower temperatures and is in between the two cases described in Ref. 23 at higher temperatures. However, the consequence of this difference is rather small for the EOS data, because we use the dissociation degree only as a factor for the vibrational energy of the molecules, which itself is small compared to the internal energy obtained by the QMD simulations.

III. EQUATION OF STATE AND HUGONIOT CURVE

We show the thermal EOS of warm dense hydrogen in Fig. 4. The isotherms of the pressure show a systematic behavior in terms of the density and temperature. We find no instability in the thermal EOS isotherms $(\partial P/\partial V)_T > 0$,

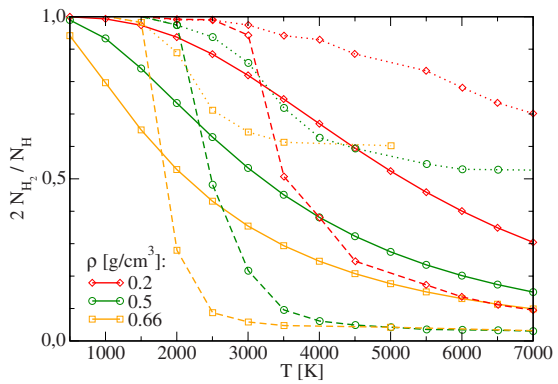

FIG. 3. (Color online) Ratio of hydrogen molecules with respect to the total number of protons for three densities: our coordination number method (solid line) is compared with the pair-counting method of Vorberger *et al.* (Ref. 23) (dotted line). Their result, which counts only pairs with a lifetime longer than ten H_2 vibrational periods, is also given (dashed line).

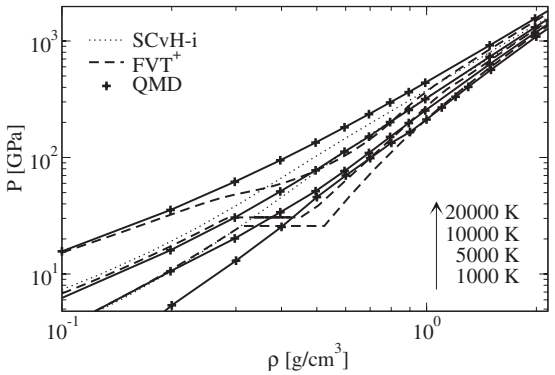

FIG. 4. Thermal EOS for warm dense hydrogen (pressure isotherms): QMD data are compared with the chemical models FVT^+ (Ref. 50) and SCvH-i (Ref. 51).

which would indicate a first order plasma phase transition (PPT). These instabilities have to be generally treated by a Maxwell construction[47] and usually occur in chemical models that use, e.g., fluid variational theory[48–50] (FVT) or liquid state perturbation theory.[51] Chemical models are based on a free energy minimization schema for a mixture of hydrogen atoms, molecules, and plasma in chemical equilibrium. Correlations are taken into account based on effective two-particle potentials. The description of the free charged particles (plasma) is done beyond the Debye–Hückel approximation by using efficient Padé formulas, which are valid for a wide region of densities and temperatures.

In Fig. 4, our QMD results are compared with the chemical model FVT[50] and that of Saumon–Chabrier–van Horn (SCvH-i).[51] The EOS derived by Saumon *et al.*[51] also showed a PPT (SCvH-PPT data set). The modified SCvH-i data set shown here avoids the PPT by using an interpolation through the instability region. Therefore, both data sets can be used to study the influence of a PPT on interior models of giant planets such as Jupiter. Consistent chemical models yield the correct low-temperature and low-density limit and agree with our QMD results there. Good agreement is also found in the high-density limit, where a nearly temperature-independent behavior characteristic of a degenerate plasma is found. At medium densities, the pressure isotherms of FVT and SCvH-i lie well below the QMD data; the deviations amount up to 25%.

We have encountered a region with $(\partial P/\partial T)_V < 0$, which was previously found.[23,24] We reproduced the isochore at $r_s = 1.75$, which was given in Ref. 23 within the uncertainties of the simulations. The instability region appears at pressures up to 200 GPa at temperatures between 1000 and 4000 K. It can be related to the rapid dissociation transition at such low temperatures, which leads to a drastic increase in the electrical conductivity (see Sec. IV). We note that an experimental signature of an instability was found in this domain[52] and that recent WPMD simulations[34] showed an instability there. We conclude that the acquisition of still more accurate EOS data for warm dense hydrogen is absolutely essential to solve this challenging problem (see also Ref. 53).

Following Lenosky *et al.*[54] and Beule *et al.*,[55] we fitted the given QMD results for the pressure P and the internal energy U by expansions in terms of density ρ and tempera-

TABLE I. Coefficients a_{ik} in the expansion for the pressure P^{int} according to Eqs. (4) and (5).

i	a_{i0}	a_{i1}	a_{i2}	a_{i3}	a_{i4}
0	0.2234	2919.84	3546.67	1.940 23	$1.113\,16\times10^{-6}$
1	14.7586	2117.98	4559.17	−17.9538	$4.880\,41\times10^{-4}$
2	−33.8469	2693.63	4159.13	70.582	-2.8848×10^{-4}

ture T. The pressure is split into ideal and interaction contributions as follows:

$$P = P^{\text{id}} + P^{\text{int}} = \frac{\rho k_B T}{m_H} + P^{\text{int}}(\rho, T). \tag{3}$$

The QMD data for the pressure P given in kilobar can be interpolated by the following expansion for the interaction contribution:

$$P^{\text{int}}(\rho, T) = [A_1(T) + A_2(T)\rho]^{A_0(T)}, \tag{4}$$

$$A_i(T) = a_{i0} \exp\left[-\left(\frac{T - a_{i1}}{a_{i2}}\right)^2\right] + a_{i3} + a_{i4}T. \tag{5}$$

The coefficients a_{ik} are summarized in Table I.

The QMD data for the specific internal energy $u = U/m$ given in kJ/g can be given by a similar expansion as follows:

$$u = \sum_{j=0}^{4} B_j(T)\rho^j, \tag{6}$$

$$B_j(T) = b_{j0} \exp\left[-\left(\frac{T - b_{j1}}{b_{j2}}\right)^2\right] + b_{j3} + b_{j4}T. \tag{7}$$

The expansion coefficients b_{jk} are given in Table II.

The expansions (4) and (6) are valid within a density range from 0.5 to 5 g/cm^3 between 500 and 20 000 K. They reproduce the *ab initio* QMD data within 5% accuracy and can easily be applied in planetary models or hydrodynamic simulations. The expansions fulfill thermodynamic consistency, which is expressed by the following relation:

$$P - T\left(\frac{\partial P}{\partial T}\right)_V = -\left(\frac{\partial U}{\partial V}\right)_T \tag{8}$$

within 15% accuracy, which is mainly due to the deviations from the QMD data itself.

TABLE II. Coefficients b_{jk} in the expansion for the specific internal energy u according to Eqs. (6) and (7).

j	b_{j0}	b_{j1}	b_{j2}	b_{j3}	b_{j4}
0	−33.8377	2154.38	3696.89	−300.446	$1.779\,56\times10^{-2}$
1	55.8794	3174.39	2571.21	56.222	$-3.562\,34\times10^{-3}$
2	−30.0376	3174.02	2794.39	87.3659	2.0819×10^{-3}
3	5.573 28	3215.51	2377.23	−13.1622	$-3.840\,04\times10^{-4}$
4	−0.3236	3245.48	2991.45	0.682 152	$2.198\,62\times10^{-5}$

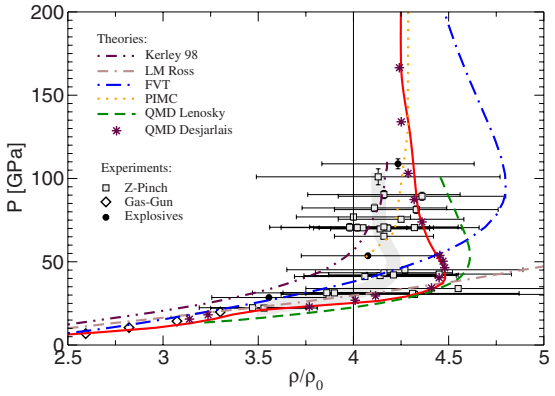

FIG. 5. (Color online) Principal Hugoniot curve for hydrogen: results of this work (solid line) are compared with previous QMD results of Lenosky *et al.* (Ref. 58) (dashed line) and Desjarlais (Ref. 22) (stars), PIMC simulations (Ref. 62) (dotted line), the linear mixing model of Ross (Ref. 60) (dot-dash-dashed line), the model EOS of Kerley (Ref. 61) (dot-dot-dashed line), and the chemical model FVT (Ref. 48) (dot-dashed line). Experiments: gas gun (Ref. 56) (diamonds), Sandia Z machine (Ref. 8) (gray squares; gray line: running average through the $u_s - u_p$ data), and high explosives (Ref. 57) (black circles).

A crucial measure for theoretical EOS data is the principal Hugoniot curve, which is plotted in Fig. 5. It describes all possible final states (ρ, P, u) of shock-wave experiments according to the following Hugoniot equation:

$$u - u_0 = \frac{1}{2}(P + P_0)\left(\frac{1}{\rho_0} - \frac{1}{\rho_0}\right), \tag{9}$$

which starts at the same initial conditions (ρ_0, P_0, u_0). For the hydrogen principal Hugoniot curve, the initial density is $\rho_0 = 0.0855$ g/cm^3 and the initial internal energy $u_0 = -314$ kJ/g at a temperature of 20 K. The initial pressure P_0 can be neglected compared to the high pressure of the final state.

Shock-wave experiments were performed for deuterium by using gas guns,[56] magnetically launched flyer plates at Sandia's Z machine,[8] or HEs.[57] These experiments indicate a maximum compression of 4.25 at about 50 GPa.

Another series of laser-driven experiments[9] shows systematic deviations from the experiments quoted above. In particular, a maximum compression of 6 has been reported at about 1 Mbar. According to the unanimous evaluation of the shock-wave experimental data for molecular liquids,[5] we compare our QMD data in Fig. 5 only with the data sets mentioned above.

The systematic increase in the cutoff energy E_{cut} in QMD simulations from 500 eV (Ref. 58) to 1200 eV (Ref. 22) has lead to fully converged results in agreement with the experimental points. The consideration of the zero-point vibrations of the H_2 molecules along the entire Hugoniot curve yields a very good agreement of QMD data with the gas gun experiments,[56] especially for lower pressures. The calculated Hugoniot curve has a maximum compression of 4.5, which is slightly higher than the HE and Z experiments indicate (about 4.25). This is an agreement of about 5% accuracy,

which can be translated into an accuracy of about 1% in the measured shock and particle velocities, which are in the range of the systematic errors in the experiments. The compression decreases with higher pressures and temperatures and reaches the correct high-temperature limit as given by the PIMC simulations.[59] The QMD curve lies slightly below the experimental data for compression rates between 3 and 4, which could be due to the known band gap problem of DFT in GGA. At a compression ratio of 3.5, the slope slightly changes due to dissociation of the molecules, which verifies earlier calculations.[24]

The FVT curve[48] is shown as a representative of chemical models which, in general, show a higher compressibility well beyond 4.5. Also shown is the linear mixing result of Ross.[60] This curve shows a sixfold compression and is not in agreement with the shown experiments. The curve of Kerley[61] has a maximum compression of 4.25, like the experiments indicate, but the pressure is there slightly higher than the results of the QMD simulations.

IV. DYNAMIC CONDUCTIVITY

The dynamic conductivity $\sigma(\omega)$ is derived from the Kubo–Greenwood formula[63,64] as follows:

$$\sigma(\omega) = \frac{2\pi e^2\hbar^2}{3m^2\omega\Omega}\sum_{\mathbf{k}} W(\mathbf{k})\sum_{j=1}^{N}\sum_{i=1}^{N}\sum_{\alpha=1}^{3}[F(\epsilon_{i,\mathbf{k}}) - F(\epsilon_{j,\mathbf{k}})] \times |\langle\Psi_{j,\mathbf{k}}|\nabla_\alpha|\Psi_{i,\mathbf{k}}\rangle|^2\delta(\epsilon_{j,\mathbf{k}} - \epsilon_{i,\mathbf{k}} - \hbar\omega), \quad (10)$$

where e is the electron charge and m is its mass. The summations over i and j run over N discrete bands considered in the electronic structure calculation for the cubic supercell volume Ω. The three spatial directions are averaged by the α sum. $F(\epsilon_{i,\mathbf{k}})$ describes the occupation of the ith band, which corresponds to the energy $\epsilon_{i,\mathbf{k}}$ and the wave function $\Psi_{i,\mathbf{k}}$ at $\mathbf{k}$. The δ function has to be broadened because a discrete energy spectrum results from the finite simulation volume.[21] An integration over the Brillouin zone is performed by sampling special $\mathbf{k}$ points,[65] where $W(\mathbf{k})$ is the respective weighting factor. We used Baldereschi's mean value point[45] to reach a convergence of better than 10% accuracy.

In Fig. 6, the dc conductivity is shown, which follows in the static limit $\omega \to 0$ from the dynamic conductivity $\sigma(\omega)$. We have performed calculations along the principal Hugoniot curve, where the dc conductivity rapidly increases, which is in very good agreement with the single shock experiments of Nellis *et al.*[14] Above 40 GPa, our results indicate a metalliclike conductivity, which is also to be seen in the reflectivity (see Fig. 7).

Weir *et al.*[15] carried out pioneering conductivity measurements with reverberating shock waves, which represent a quasi-isentropic compression so that higher densities could be reached at lower temperatures. We show three relevant QMD isotherms between 1000 and 2000 K in Fig. 6 and find qualitative agreement with these experiments and previous QMD simulations of Collins *et al.*,[12] particularly a transition to a metallic fluid above 1 Mbar is observed.

Optical properties can be derived from the frequency-dependent conductivity $\sigma(\omega)$ [see Eq. (10)]. The standard

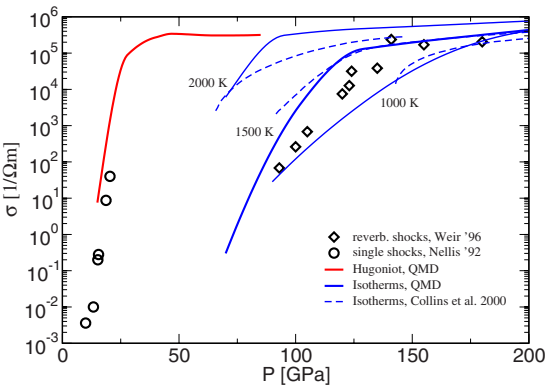

FIG. 6. (Color online) dc conductivity for hydrogen: QMD results along the Hugoniot curve and along three isotherms are compared with the single shock data of Nellis *et al.* (Ref. 14) and multiple shock data of Weir *et al.* (Ref. 15). Earlier QMD results of Collins *et al.* (Ref. 12) are also shown.

method is to obtain the imaginary part via the Kramers–Kronig relation as follows:

$$\sigma_2(\omega) = -\frac{2}{\pi}\mathrm{P}\int\frac{\sigma_1(\nu)\omega}{(\nu^2-\omega^2)}d\nu, \quad (11)$$

where P is the principal value of the integral. The dielectric function can be directly calculated by using the conductivity as follows:

$$\epsilon_1(\omega) = 1 - \frac{1}{\epsilon_0\omega}\sigma_2(\omega), \quad (12)$$

$$\epsilon_2(\omega) = \frac{1}{\epsilon_0\omega}\sigma_1(\omega). \quad (13)$$

The square of the index of refraction, which contains the real part n and the imaginary part k, is equal to the dielectric function, which leads to the following relations:

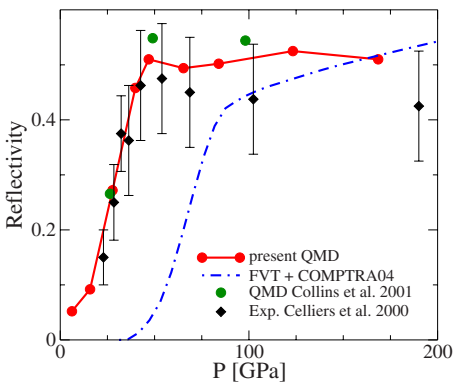

FIG. 7. (Color online) Reflectivity for a wavelength of 808 nm along the Hugoniot curve of hydrogen: QMD results are compared with the experimental data of Celliers *et al.* (Ref. 66) and predictions of the chemical model FVT (Ref. 67) by using the COMPTRA code (Ref. 68) and QMD simulations of Collins *et al.* (Ref. 20).

$$n(\omega) = \sqrt{\tfrac{1}{2}[|\epsilon(\omega)| + \epsilon_1(\omega)]}, \tag{14}$$

$$k(\omega) = \sqrt{\tfrac{1}{2}[|\epsilon(\omega)| - \epsilon_1(\omega)]}. \tag{15}$$

The index of refraction is then used to calculate optical properties such as the reflectivity r,

$$r(\omega) = \frac{[1 - n(\omega)]^2 + k(\omega)^2}{[1 + n(\omega)]^2 + k(\omega)^2}. \tag{16}$$

We compare our *ab initio* results with the reflectivities measured along the Hugoniot curve[66] in Fig. 7. The agreement is excellent, as well as with some earlier QMD data points.[20] The change in hydrogen reflectivity with pressure can be interpreted as a gradual transition from a molecular insulating fluid through an atomic fluid at above 20 GPa, where the atoms have strongly fluctuating bonds with next neighbors[20] to a dense, almost fully ionized plasma with a reflectivity of about 50–60% at high pressures above 40 GPa. The chemical model[67] shows the same behavior, but the abrupt increase in reflectivity occurs at a higher density. This shows the difficulties of using chemical models in finding the correct shifts of the dissociation and ionization energies as functions of density and temperature and, thus, the location of the nonmetal-to-metal transition.

V. CONCLUSION

We have performed *ab initio* QMD simulations to study the thermophysical properties of hydrogen under extreme conditions. As a result, we obtained highly converged EOS data, which are relevant for modeling giant planets and for the understanding of the fundamental behavior of hydrogen at high pressure. The deviations between our QMD data and chemical models amount up to 25%. We have constructed smooth fit functions for the QMD data for the pressure and the internal energy, which can be easily used in, e.g., hydrodynamic simulations for warm dense hydrogen and in astrophysical applications. The results show a smooth transition from a molecular liquid to an atomic fluid of metal-like state. We have calculated the principal Hugoniot curve, which is in agreement with dynamic experiments and has the correct high-temperature limit as given by PIMC simulations. We have derived the optical properties by using the Kubo–Greenwood formula. The reflectivity along the Hugoniot curve is in excellent agreement with experiments. The results show a nonmetal-to-metal transition at about 40 GPa, which is in accordance with the dc electrical conductivity data. The accurate description of warm dense hydrogen for off-Hugoniot states reached, e.g., by quasi-isentropic compression remains a challenging problem.

ACKNOWLEDGMENTS

We thank P. M. Celliers, W. Ebeling, V. E. Fortov, M. French, A. Höll, A. Kietzmann, W. D. Kraeft, T. R. Mattsson, B. Militzer, V. B. Mintsev, N. Nettelmann, H. Reinholz, G. Röpke, N. A. Tahir, V. Ya. Ternovoi, C. Toepffer, and G. Zwicknagel for stimulating discussions and for providing us with their data. This work was supported by the Deutsche Forschungsgemeinschaft within SFB 652 and by the High Performance Computing Center North (Grant No. mvp00006). We acknowledge the support of the computer center of the University of Rostock. Sandia is a multiprogram laboratory operated by Sandia Corporation, a Lockheed Martin Co., for the U.S. Department of Energy National Nuclear Security Administration under Contract No. DE-AC04-94AL85000.

[1] T. Guillot, Science **286**, 72 (1999).
[2] T. Guillot, Planet. Space Sci. **47**, 1183 (1999).
[3] J. D. Lindl, P. Amendt, R. L. Berger, S. G. Glendinning, S. H. Glenzer, S. W. Haan, R. L. Kauffman, O. L. Landen, and L. J. Suter, Phys. Plasmas **11**, 339 (2004).
[4] V. B. Mintsev and V. E. Fortov, J. Phys. A **39**, 4319 (2006).
[5] W. J. Nellis, Rep. Prog. Phys. **69**, 1479 (2006).
[6] M. D. Knudson, D. L. Hanson, J. E. Bailey, C. A. Hall, J. R. Asay, and W. W. Anderson, Phys. Rev. Lett. **87**, 225501 (2001).
[7] M. D. Knudson, D. L. Hanson, J. E. Bailey, C. A. Hall, and J. R. Asay, Phys. Rev. Lett. **90**, 035505 (2003).
[8] M. D. Knudson, D. L. Hanson, J. E. Bailey, C. A. Hall, J. R. Asay, and C. Deeney, Phys. Rev. B **69**, 144209 (2004).
[9] R. Cauble *et al.*, Phys. Plasmas **4**, 1857 (1997).
[10] D. M. Ceperley and E. Manousakis, J. Chem. Phys. **115**, 10111 (2001).
[11] K. T. Delaney, C. Pierleoni, and D. M. Ceperley, Phys. Rev. Lett. **97**, 235702 (2006).
[12] L. A. Collins, J. D. Kress, S. R. Bickham, T. J. Lenosky, and N. J. Troullier, High Press. Res. **16**, 313 (2000).
[13] L. A. Collins, I. Kwon, J. D. Kress, N. J. Troullier, and D. Lynch, Phys. Rev. E **52**, 6202 (1995).
[14] W. J. Nellis, A. C. Mitchell, P. C. McCandless, D. J. Erskine, and S. T. Weir, Phys. Rev. Lett. **68**, 2937 (1992).
[15] S. T. Weir, A. C. Mitchell, and W. J. Nellis, Phys. Rev. Lett. **76**, 1860 (1996).
[16] W. J. Nellis, S. T. Weir, and A. C. Mitchell, Phys. Rev. B **59**, 3434 (1999).
[17] R. Redmer, High Press. Res. **16**, 345 (2000).
[18] R. Redmer, G. Röpke, S. Kuhlbrodt, and H. Reinholz, Phys. Rev. B **63**, 233104 (2001).
[19] T. J. Lenosky, J. D. Kress, L. A. Collins, and I. Kwon, Phys. Rev. B **55**, R11907 (1997).
[20] L. A. Collins, S. R. Bickham, J. D. Kress, S. Mazevet, T. J. Lenosky, N. J. Troullier, and W. Windl, Phys. Rev. B **63**, 184110 (2001).
[21] M. P. Desjarlais, J. D. Kress, and L. A. Collins, Phys. Rev. E **66**, 025401(R) (2002).
[22] M. P. Desjarlais, Phys. Rev. B **68**, 064204 (2003).
[23] J. Vorberger, I. Tamblyn, B. Militzer, and S. A. Bonev, Phys. Rev. B **75**, 024206 (2007).
[24] S. A. Bonev, B. Militzer, and G. Galli, Phys. Rev. B **69**, 014101

(2004).
[25] S. Mazevet, J. D. Kress, L. A. Collins, and P. Blottiau, Phys. Rev. B **67**, 054201 (2003).
[26] Y. Laudernet, J. Clérouin, and S. Mazevet, Phys. Rev. B **70**, 165108 (2004).
[27] S. Mazevet, M. P. Desjarlais, L. A. Collins, J. D. Kress, and N. H. Magee, Phys. Rev. E **71**, 016409 (2005).
[28] S. Mazevet, F. Lambert, F. Bottin, G. Zérah, and J. Clérouin, Phys. Rev. E **75**, 056404 (2007).
[29] D. Klakow, C. Toepffer, and P.-G. Reinhard, J. Chem. Phys. **101**, 10766 (1994).
[30] S. Nagel, R. Redmer, G. Röpke, M. Knaup, and C. Toepffer, Phys. Rev. E **57**, 5572 (1998).
[31] M. Knaup, P.-G. Reinhard, and C. Toepffer, Contrib. Plasma Phys. **39**, 57 (1999).
[32] M. Knaup, G. Zwicknagel, P.-G. Reinhard, and C. Toepffer, Nucl. Instrum. Methods Phys. Res. A **464**, 267 (2001).
[33] M. Knaup, P.-G. Reinhard, C. Toepffer, and G. Zwicknagel, J. Phys. A **36**, 6165 (2003).
[34] B. Jakob, P.-G. Reinhard, C. Toepffer, and G. Zwicknagel, Phys. Rev. E **76**, 036406 (2007).
[35] A. E. Mattsson, P. A. Schultz, M. P. Desjarlais, T. R. Mattsson, and K. Leung, Modell. Simul. Mater. Sci. Eng. **13**, R1 (2005).
[36] P. Hohenberg and W. Kohn, Phys. Rev. **136**, B864 (1964).
[37] W. Kohn and L. J. Sham, Phys. Rev. **140**, A1133 (1965).
[38] N. D. Mermin, Phys. Rev. **137**, A1441 (1965).
[39] G. Kresse and J. Hafner, Phys. Rev. B **47**, 558 (1993).
[40] G. Kresse and J. Hafner, Phys. Rev. B **49**, 14251 (1994).
[41] G. Kresse and J. Furthmüller, Phys. Rev. B **54**, 11169 (1996).
[42] G. Kresse and D. Joubert, Phys. Rev. B **59**, 1758 (1999).
[43] J. P. Perdew, K. Burke, and M. Ernzerhof, Phys. Rev. Lett. **77**, 3865 (1996).
[44] S. Nosé, J. Chem. Phys. **81**, 511 (1984).
[45] A. Baldereschi, Phys. Rev. B **7**, 5212 (1973).
[46] A. Kietzmann, B. Holst, R. Redmer, M. P. Desjarlais, and T. R. Mattsson, Phys. Rev. Lett. **98**, 190602 (2007).
[47] D. Beule, W. Ebeling, A. Förster, H. Juranek, R. Redmer, and G. Röpke, Phys. Rev. E **63**, 060202(R) (2001).
[48] H. Juranek and R. Redmer, J. Chem. Phys. **112**, 3780 (2000).
[49] H. Juranek, R. Redmer, and Y. Rosenfeld, J. Chem. Phys. **117**, 1768 (2002).
[50] B. Holst, N. Nettelmann, and R. Redmer, Contrib. Plasma Phys. **47**, 368 (2007).
[51] D. Saumon, G. Chabrier, and H. M. van Horn, Astrophys. J., Suppl. Ser. **99**, 713 (1995).
[52] V. E. Fortov *et al.*, Phys. Rev. Lett. **99**, 185001 (2007).
[53] S. A. Bonev, E. Schwegler, T. Ogitsu, and G. Galli, Nature (London) **431**, 669 (2004).
[54] T. J. Lenosky, J. D. Kress, and L. A. Collins, Phys. Rev. B **56**, 5164 (1997).
[55] D. Beule, W. Ebeling, A. Förster, H. Juranek, S. Nagel, R. Redmer, and G. Röpke, Phys. Rev. B **59**, 14177 (1999).
[56] W. J. Nellis, A. C. Mitchell, M. van Thiel, G. J. Devine, R. J. Trainor, and N. Brown, J. Chem. Phys. **79**, 1480 (1983).
[57] G. V. Boriskov, A. I. Bykov, R. Ilkaev, V. D. Selemir, G. V. Simakov, R. F. Trunin, V. D. Urlin, A. N. Shuikin, and W. J. Nellis, Phys. Rev. B **71**, 092104 (2005).
[58] T. J. Lenosky, S. R. Bickham, J. D. Kress, and L. A. Collins, Phys. Rev. B **61**, 1 (2000).
[59] B. Militzer, D. M. Ceperley, J. D. Kress, J. D. Johnson, L. A. Collins, and S. Mazevet, Phys. Rev. Lett. **87**, 275502 (2001).
[60] M. Ross, Phys. Rev. B **58**, 669 (1998).
[61] G. I. Kerley, Sandia National Laboratories Technical Report No. SAND2003-3613, 2003.
[62] B. Militzer and D. M. Ceperley, Phys. Rev. Lett. **85**, 1890 (2000).
[63] R. Kubo, J. Phys. Soc. Jpn. **12**, 570 (1957).
[64] D. A. Greenwood, Proc. Phys. Soc. London **71**, 585 (1958).
[65] H. J. Monkhorst and J. D. Pack, Phys. Rev. B **13**, 5188 (1976).
[66] P. M. Celliers, G. W. Collins, L. B. DaSilva, D. M. Gold, R. Cauble, R. J. Wallace, M. E. Foord, and B. A. Hammel, Phys. Rev. Lett. **84**, 5564 (2000).
[67] R. Redmer, H. Juranek, N. Nettelmann, and B. Holst, in *Shock Compression of Condensed Matter—2005*, AIP Conf. Proc. No. 845, edited by M. D. Furnish, M. Elert, T. P. Russell, and C. T. White (AIP, Melville, NY, 2006), pp. 127–130.
[68] S. Kuhlbrodt, B. Holst, and R. Redmer, Contrib. Plasma Phys. **45**, 73 (2005). The COMPTRA04 source code and data files can be found at http://www.physik.uni-rostock.de/statphys/pages/comptra.